Electric Power Systems Research 217 (2023) 109120

Contents lists available at ScienceDirect

Electric Power Systems Research

journal homepage: www.elsevier.com/locate/epsr

Reinforcement of the distribution grids to improve the hosting capacity of distributed generation: Multi-objective framework

Bahman Ahmadi [a], Oguzhan Ceylan [b], Aydogan Ozdemir [c,*]

[a] Department of Electrical Engineering, Mathematics and Computer Science, University of Twente, Enschede, Netherlands
[b] Department of Electrical and Electronics Engineering, Marmara University, Istanbul, Turkey
[c] Department of Electrical Engineering, Istanbul Technical University, Istanbul, Turkey

ARTICLE INFO

Keywords:
Distributed generation
Hosting capacity
Energy storage systems
Static var compensator
Multi-objective optimization

ABSTRACT

Excessive penetration of renewable energy resources into the distribution grid without additional preventive measures has led to several operational problems. However, most strategies developed to accommodate more renewable energy units suffered from other operational problems. Therefore, further efforts are needed to address the other key vulnerabilities of the grid in addition to maximizing the hosting capacity. In this regard, this study is devoted to a new multi-objective formulation to maximize the hosting capacity and minimize the total energy losses while satisfying the operational constraints and maximizing the energy transferred to off-peak hours. The Multi-Objective Advanced Gray Wolf Optimization (MOAGWO) algorithm is used as a solution tool. The proposed formulation and solution algorithm are tested on IEEE-33-bus and 69-bus medium voltage test systems. The impacts of energy storage systems, voltage regulators, and static var compensators on the hosting capacity and the objective functions are identified using several scenarios. The results showed that the optimal device type and locations depend on the level of DG penetration. Finally, a comparison according to two popular multi-objective performance indices showed that the quality of the Pareto front distribution obtained by MOAGWO was better than the ones obtained with the two other popular heuristic methods.

1. Introduction

The growth in the penetration of distributed generation (DG) units into electricity distribution networks (EDNs) has been driven by their economic benefits, low environmental impacts, and reduced reliance on fossil fuels. However, excessive integration of these units without additional preventive measures can lead to various operational problems, such as overvoltages, power quality issues, low reliability, low customer satisfaction [1], excessive line losses, overloading of transformers and feeders, protection failures, and high harmonic distortion levels that exceed the limits of international standards. Therefore, the network operator should look to enhance existing power generation plants and distribution capabilities [2] besides the relevant planning and operational strategies to maximize the integration of DG units through the proper use of these technologies. Under this premise, the concept of analyzing the hosting capacity of EDNs was born. A distribution grid's DG hosting capacity (DGHC) is defined as the maximum amount of DG that can be integrated into the grid without creating any voltage magnitude, protection, and power quality problems [3].

Emerging technologies and techniques to improve DGHC include the use of smart inverters [4,5], energy storage systems (ESSs) [6,7], static var compensators (SVC) [8], power curtailment of DGs [9,10], passive harmonic filters [11], on-load tap-changers (OLTCs) [12], capacitor banks [13], and demand response adaptation [14,15]. Much has been written in the literature on how to incorporate the above devices into power grids to increase the hosting capacity.

DGHC analysis for single or multiple types of DG units has been addressed using a variety of approaches. Liu et al. developed a stochastic framework for single and hybrid DGHC and applied it in IEEE 33-bus medium voltage (MV) system [16]. Liu et all. proposed a sensitivity region-based optimization method to maximize the renewable generation hosting capacity of an islanded microgrid [17]. In [18], the impact of high electric vehicle (EV) penetration on the DGHC of EDNs was evaluated. Optimal planning of storage devices to increase the DGHC was presented in [19]. In [20], a new formulation for maximizing the hosting capacity of PV systems considering dynamic reactive control of smart inverters was proposed. The improvement of the hosting capacity of multi-wind turbine systems (WT) with the proper operation of OLTC and voltage regulators (VR) was presented in [21]. Moreover, the charging management of EVs was included in the process to regulate the WT generation.

* Corresponding author.
E-mail addresses: b.ahmadi@utwente.nl (B. Ahmadi), oguzhan.ceylan@marmara.edu.tr (O. Ceylan), ozdemiraydo@itu.edu.tr (A. Ozdemir).

https://doi.org/10.1016/j.epsr.2023.109120
Received 7 October 2022; Received in revised form 18 December 2022; Accepted 5 January 2023
Available online 10 January 2023
0378-7796/© 2023 The Authors. Published by Elsevier B.V. This is an open access article under the CC BY license (http://creativecommons.org/licenses/by/4.0/).

Until now, most research has focused on estimating the maximum capacity of DG penetration in the system or utilizing the other devices that increase DGHC. However, more efforts are needed to address the other major weaknesses of EDNs in addition to DGHC maximization. Therefore, this paper focuses on a multi-objective formulation based on the concept of optimal Pareto front [22] to maximize the DGHC while minimizing the total energy losses and maximizing the energy transferred to off-peak hours.

We have attempted to identify the effects of various devices on DGHC in EDNs. At this point, ESSs, voltage regulators (VR), and SVCs are considered to increase the HC while coordinating voltage profiles and reducing energy losses. In addition, the energy transferred to off-peak hours is maximized by the optimal control strategy of the ESS units. It was not held as an objective function because some of the scenarios did not comprise the ESS units. The number, size, and location of the two popular types of DG units, PV and WT, are optimized within a multi-objective optimization cycle. Different scenarios are proposed to determine the impacts of the ESS, VR, and SVC units on the two objectives, namely, maximization of DGHC and minimization of energy losses.

Heuristic optimization algorithms are designed in all forms, from simple "trial and error" to complex ones based on mimicking natural environmental conditions. The strategies of the algorithms are easy to understand and simple to implement. In [23–26], several heuristic algorithms were used to improve the hosting capacity of EDNs. Based on the results found in the literature, the objective function of the optimization process was formulated to maximize the DG capacity integrated into a system without any voltage violation. The weakest point of that single-objective formulation was the need to consider other prospective concerns of the system.

In this study, the Multi-Objective Advanced Grey Wolf Optimization (MOAGWO) Algorithm [27] is used to determine the Pareto-optimal front solutions for several scenarios of maximizing the DGHC using the ESS, SVCs, and VR while minimizing the active energy losses of the networks. MOAGWO is a multi-objective optimization algorithm developed to improve the Grey Wolf optimization (GWO) algorithm's base search capability and convergence performance. The main modifications over the base GWO method consist of applying a dynamic method to evaluate the wolf positions, either in the exploration or the exploitation phase of the optimization process. Additionally, the mirroring distance concept is used to update the search agents' positions, ensuring that the positions always remain within the feasible range. The new formulations for updating the positions of the wolves in MOAGWO improved the simulation time and increased the robustness of the method in finding near-optimal solutions and not falling into the local minimas in the search space. The proposed formulation and solution algorithm are tested on IEEE-33-bus and 69-bus test systems. The quality of the results is validated by comparing the Pareto solutions and the computational burden of MOAGWO with the other known methods.

The main contributions of the paper are as follows:

- A new multi-objective formulation is proposed to maximize the hosting capacity and minimize the total energy losses,
- The energy transferred to the off-peak hours, formulated as a constraint, is also maximized through the optimal control strategy of ESS units,
- The Multi-Objective Advanced Grey Wolf Optimization (MOAGWO) algorithm is adapted to determine the Pareto front solutions.
- The singular and collaborative impacts of the reinforcement units on the objectives are identified and several solutions are proposed for different DG penetration levels.
- The quality of the results are validated by comparing the Pareto solutions and the computational efficiency of MOAGWO with other known methods.

The structure of the paper is as follows. The statement of the problem, including the objective functions and constraints, is described in Section 2. Section 3 is devoted to the MOAGWO method and its implementation for the multi-objective optimization problem. Section 4 shows the simulation results for test system applications. Conclusions are summarized in Section 5.

2. Multi-objective formulation of the problem

The proposed two-dimensional objective function of the study includes the DGHC and total energy loss expressions. They are considered separate objectives and optimized by the Pareto optimum concept in the multi-objective optimization procedure.

2.1. Objective functions

A detailed formulation of the objective functions is elaborated in the following sections.

2.1.1. Total energy losses

Real power losses in jth branch of a distribution network at hour-i can be calculated as $Pl_j^i = (I_j^i)^2.R_j$, where R_j is the resistance of the jth branch. Energy losses are the sum of hourly power losses for an intended period (N_T). Total energy losses of the system with N_{br} branches, f_{TEL}, can be expressed as the sum of hourly losses over an optimization period of N_T hours as follows:

$$f_{\text{TEL}} = \sum_{i=1}^{N_T} \sum_{j=1}^{N_{br}} Pl_j^i \tag{1}$$

Note that f_{TEL} shows the annual energy losses if the optimization period is a year.

2.1.2. Distributed generation hosting capacity

The hosting capacity for a grid comprising DG units is defined as the maximum amount of DG capacity (size) that can be integrated into the grid without creating any voltage magnitude. Here the goal for the objective function is to increase the hosting capacity of the DG units, so the objective function variables are defined as the size of individual units in the grid beside the number of voltage violations in the system. In the minimization objective function modeling, one way is to have a term in the formulation for the size of the DG units and another term for the violations as the penalty function. In this study, a new formulation was proposed for the DGHC of the network:

$$f_{\text{DGHC}} = \frac{1 + \sum_{i=1}^{N_T} (\sum_{j=1}^{N_{BUS}} K_j^i)}{\sum_{n=1}^{N_{PV}} S_{PV_n} + \sum_{m=1}^{N_{WT}} S_{WT_m}} \tag{2}$$

with

$$K_j^i = \begin{cases} 0, & \text{if } 0.95V_{ref} < V_j^i < 1.05V_{ref} \\ b \times (2 - \frac{t}{Max_t}), & \text{otherwise} \end{cases} \tag{3}$$

where N_{BUS} is the number of busses in the feeder, and V_j^i is the jth bus voltage magnitude at hour-i, calculated by forward/backward sweep (FBS) power flow [28] method. The reference voltage (V_{ref}) is assumed as 1 p.u. N_{PV} and N_{WT} represent the number of PV and WT units found in the optimization process with the unit size of S_{PV} and S_{WT}. The maximum number of iterations in the optimization process and the current iteration are shown with Max_t and t, respectively. A constant quantity b is used in a penalty term for the voltage magnitude violations.

Note that the objective function aims to increase the capacity of the DG units without voltage violations. Therefore the K at the end is expected to be zero.

2.2. Constraints

The equality and inequality constraints comprising the power balance equations and the physical constraints on the electrical parameters are described below.

1 Power balance: Generated power should be equal to the sum of the consumed power and the losses at each hour of the simulation period.

$$P^i_{\mathrm{MG}} + P^i_{\mathrm{DG}} + P^i_{\mathrm{ESSD}} = P^i_{\mathrm{load}} + P^i_{\mathrm{ESSC}} + P^i_{\mathrm{losses}}, \forall i \in N_{\mathrm{t}} \quad (4)$$

$$Q^i_{\mathrm{MG}} = Q^i_{\mathrm{load}} + Q^i_{\mathrm{losses}}, \forall i \in N_{\mathrm{t}} \quad (5)$$

where P_{MG} and Q_{MG} are the active and reactive power supplied from the main grid at the slack bus. N_t is a set of $\{1, 2, 3, \ldots, N_T\}$ representing time periods. P_{DG} shows the total active power generated by DGs. P_{ESSD} and P_{ESSC} denote discharge and charge powers of ESS units, respectively. Active and reactive loads and losses are represented by P_{load}, Q_{losses}, Q_{load} and Q_{losses}, respectively.

2 Bus voltage magnitude limits: In order to maintain power quality, the node voltages should be within operation limits as shown below.

$$V_j^{i,\min} \le V_j^i \le V_j^{i,\max} \quad \forall i \in N_{\mathrm{T}}, j \in N_{\mathrm{Bus}} \quad (6)$$

where the values of $V_j^{i,\max}$ and $V_j^{i,\min}$ are assigned as 1.05 and 0.95 p.u. in this study, respectively

3 Generation constraints: The upper limit of DG active power outputs are assumed to be 1 MW due to the governmental incentives provided for small-scale DG units in Turkey. On the other hand, the main grid supply is limited due to generation and load profiles at each hour.

$$P^i_{\mathrm{MG}} \le P_{\mathrm{MG}_{max}}, \forall i \in N_{\mathrm{T}} \quad (7)$$

$$Q^i_{\mathrm{MG}} \le Q_{\mathrm{MG}_{max}}, \forall i \in N_{\mathrm{T}} \quad (8)$$

$$P_{\mathrm{DG}} \le P_{\mathrm{DG}_{max}} \quad (9)$$

4 Storage constraints: The upper limit for ESS energy sizes are set as 1 MWh, while their charging/discharging amounts are restricted at each time step to limit the state of charge (SoC) of the units. The constraints of ESS units are formulated as follows.

$$\mathrm{E_{ESS}} \le \mathrm{E_{ESS}}_{max} \quad (10)$$

$$(P^i_{ESSC}, P^i_{ESSD}) \le 1MW, \forall i \in N_{\mathrm{T}} \quad (11)$$

$$0.2 * E_{ESS} \le SOC^i_{ESS} \le 0.8 * E_{ESS}, \forall i \in N_{\mathrm{T}} \quad (12)$$

Maximizing the energy transferred to off-peak hours through the optimal control strategy of the ESS units is added as a constraint for the problem. The constraint function to improve the energy transfer (of the ESS output) between peak and off-peak hours is expressed as,

$$PF = \sum_{n=1}^{N_{ESS}} \sum_{i=1}^{N_T} \left(\frac{\rho_D}{P^n_{ESSD_i}} + \frac{\rho_C}{P^n_{ESSC_i}} \right) \quad (13)$$

where P_{ESSD} and P_{ESSC} represent ESS discharge and charge powers, respectively. The control strategy for charging and discharging powers of ESS units are identified by binary decision variables ρ_C and ρ_D as follows:

$$\forall P^i_{\mathrm{load}} < \underline{P}, \exists \{\rho_C = 1, \rho_D = 0\} \quad (14)$$

$$\forall P^i_{\mathrm{load}} > \overline{P}, \exists \{\rho_C = 0, \rho_D = 1\} \quad (15)$$

$$\forall \underline{P} \le P^i_{\mathrm{load}} \le \overline{P}, \exists \{\rho_C = 0, \rho_D = 0\} \quad (16)$$

where P^i_{load} is the net active load at ith hour, and $\underline{P}$ and $\overline{P}$ are defined as:

$$\overline{P} = (P^{\mathrm{mean}}_{\mathrm{load}} + P^{\mathrm{std.}}_{\mathrm{load}}) \quad (17)$$

$$\underline{P} = (P^{\mathrm{mean}}_{\mathrm{load}} - P^{\mathrm{std.}}_{\mathrm{load}}) \quad (18)$$

where $P^{\mathrm{mean}}_{\mathrm{load}}$ and $P^{\mathrm{std.}}_{\mathrm{load}}$ are the daily average and the standard deviation of the hourly loads, respectively.

5 SVC units constraints: The amount of absorption or injection of reactive power for each time step is the control each parameter of SVCs, and the absolute amount of absorption or injection limits the SVC size as shown below.

$$S_{SVC} \le S_{SVC_{max}} \quad (19)$$

$$-S_{SVC} \le Q^i_{SVC} \le S_{SVC}, \forall i \in N_{\mathrm{T}} \quad (20)$$

where maximum SVC size is set to 0.2 MVAr, and at each time step SVC controller can absorb or inject the reactive power within −0.2 to 0.2 MVAr.

6 Voltage regulator constraints: In the simulations, we assume that the VR is located between bus 1 and 2. The allowable range for the tap position of the VRs is assumed to be $-16 \le Tap \le 16$, with the minimum and maximum tap positions corresponding to −5% and +5% of the rated voltage, respectively. The other constraints of the VR units can be found in [29].

2.3. Problem formulation

Based on the objectives and constraints discussed in the previous subsection, the formulation of the multi-objective optimization model is framed in Eq. (21).

$$\underset{w.r.t. \quad \vec{X}}{\mathrm{Minimize}} \quad F(\vec{X}) = \{f_{\mathrm{TEL}}, f_{\mathrm{DGHC}}\} \quad (21)$$

$$\vec{X} = \{\vec{L}, \vec{S}, \overrightarrow{Type}, \vec{E}, \vec{P}, \vec{O}, \overrightarrow{\mathrm{Tap}}\}$$

$$\text{Subject to} \begin{cases} g_n \ge 0, & n = 1, 2, \ldots, p \\ h_n = 0, & n = 1, 2, \ldots, q \end{cases}$$

where $\vec{L}$ is a common location vector for all devices, $\vec{S}$ is a size vector for DG and SVCs, and $\vec{O}$ denotes the operation strategy vector for ESSs and SVCs. The remaining vectors $\overrightarrow{Type}$, $\vec{E}$, and $\vec{P}$ denote the type of the DG (PV or WT), energy (size) of ESS units, and maximum charging/discharging power of ESS units, respectively. Finally, $\overrightarrow{\mathrm{Tap}}$ shows the tap position of the VR. Note that the upper and lower limits of the control variables for each test system are defined in the following sections. The terms h_n and g_n denote the equality and inequality constraints, respectively.

3. Solution methodology

3.1. Multi-objective optimization problems

The mathematical formulation of an n-dimensional multi-objective optimization problem can be given as follows:

$$\underset{w.r.t. \quad \vec{X}}{\mathrm{Minimize}} \quad F(\vec{X}) = \{f_1(\vec{X}), f_2(\vec{X}), \ldots, f_n(\vec{X})\} \quad (22)$$

$$\vec{X} = \{x_1, x_2, \ldots, x_d\}$$

$$\text{Subject to} \begin{cases} g_t(\vec{X}) \ge 0, t = 1, 2, \ldots, p \\ h_t(\vec{X}) = 0, t = 1, 2, \ldots, q \\ (\vec{X})^{lb} \le \vec{X} \le (\vec{X})^{ub} \end{cases}$$

where a set of solutions can be found for n individual objective functions and d control variables as an acceptable trade-off instead of an optimal solution. Note that $(\vec{x})^{lb}$ and $(\vec{x})^{ub}$ denote the lower and the upper bound of the control variable $\vec{x}$, respectively. The optimal solutions can be characterized by dominance relations, Pareto efficiency, and optimality definitions [30].

3.2. Multi-objective Advanced Grey Wolf Algorithm (MOAGWO)

The AGWO algorithm [27] was proposed to improve the simulation speed and convergence performance of the basic GWO [31]. An important modification is the application of a dynamic method to evaluate the wolves' positions during the exploration and exploitation phases of the process. Moreover, mirroring distances are used to update the positions of the search agents, ensuring that they are always within feasible ranges [27]. MOAGWO is the multi-objective version of the AGWO algorithm modified for finding the Pareto optimal solutions in a multi-objective optimization problem. Based on the Pareto dominance, Pareto optimality, and Pareto optimal set definitions [32], the development of the multi-objective version of AGWO is explained below.

In order to mathematically formulate the hunting process by a group of N wolves, each wolf location can be estimated by d variables. The position variables (location of the wolf) change considering the positions of the hunting leaders (α, β, and δ wolves) using the three phases of encircling, hunting, and attacking prey. At first, a random location for the wolves is generated, and the closest wolves (non-dominated solutions) to the prey(s) are stored in a repository called an archive. Each hunter will update its location based on the location of randomly chosen leaders from the archive repository. At each iteration, the location of the leaders to be followed is presented by $\vec{X}_\alpha$, $\vec{X}_\beta$, and $\vec{X}_\delta$. The algorithm updates the location of the wolves considering the boundaries of the search space around the leader(s) location using the following formulation. More information about updating the positions are given in [27].

$$\vec{X}_1 = \vec{X}_\alpha - \vec{A}_1.|\vec{B}_1.\vec{X}_\alpha - \vec{X}| \tag{23}$$

$$\vec{X}_2 = \vec{X}_\beta - \vec{A}_2.|\vec{B}_2.\vec{X}_\beta - \vec{X}| \tag{24}$$

$$\vec{X}_3 = \vec{X}_\delta - \vec{A}_3.|\vec{B}_3.\vec{X}_\delta - \vec{X}| \tag{25}$$

$$\vec{X}_4 = \vec{X} + (2.a.\vec{r}_1 - a) \times sin(2\pi\vec{r}_2).|\vec{B}_4.\vec{X}_\alpha - \vec{X}| \tag{26}$$

$$\vec{X}_5 = \vec{X} + (2.a.\vec{r}_3 - a) \times cos(2\pi\vec{r}_4).|\vec{B}_5.\vec{X}_\alpha - \vec{X}| \tag{27}$$

$$\vec{A} = (2.a.\vec{r}_5 - a) \times (sin(2\pi\vec{r}_6)) \tag{28}$$

$$\vec{B} = 2.\vec{r}_7 \tag{29}$$

$$a = 2 - 2 \times \frac{t}{\mathrm{Max}_t} \tag{30}$$

$$\vec{X}_{(t+1)} = \begin{cases} \frac{\vec{X}_1+\vec{X}_2+\vec{X}_3}{3} & r_8 \geq 1 - \frac{t}{\mathrm{Max}_t} \\ \begin{cases} \vec{X}_4 & r_9 < 0.5 \\ \vec{X}_5 & r_9 \geq 0.5 \end{cases} & r_8 < 1 - \frac{t}{\mathrm{Max}_t} \end{cases} \tag{31}$$

where $\vec{X}$ shows the location of each iteration in tth iteration, a linearly decreases from 2 to 0 over the course of iterations, and simulates the behavior of chasing a prey by the wolves. The maximum number of the iterations for the hunting process is set to Max_t, the terms $\vec{r}_1$ to $\vec{r}_7$ are random vectors between zero to one and r_8 and r_9 are random numbers within zero to one.

Depending on the value of $\vec{A}$, each wolf can either attack the prey or search for another prey in the search space. The dual behavior improves the exploration phase of the algorithm since, in the first iteration, the chance of searching for new prey is high. At the final iteration, the value of $\vec{A}$ will be close to zero, and it will simulate the behavior of catching prey by the wolves.

After updating the locations of the wolves based on the selected leaders from the archive repository, non-dominated solutions from the new locations of the wolves and the stored solutions in the archive (based on objective values of the locations) will be stored in the archive.

To find more accurate Pareto solutions, a dynamic termination criterion is added to the algorithm based on the percentage of dominance. The percentage of dominance when comparing the stored solution of the archive in the current iteration of the process with a given iteration number is added as a second termination criterion. The optimization process stops when the percentage is smaller than a pre-specified value. The mathematical formulation of the stopping criteria is given in Eq. (32).

$$B_{stop} = \begin{cases} \text{stop} & if \quad |C(t, t-a)| < \epsilon \\ \text{next iteration} & \text{otherwise} \end{cases} \tag{32}$$

where B_{stop} is used for the stopping process, ϵ is a pre-specified small number denoting a tolerance, t and a are the current iteration number and a predefined integer number for the comparison of the solutions with DP index [33].

Beside the stopping criteria, a mirroring method used to check the locations of the wolves to be within the boundaries [27]. The algorithm of the hunting process is shown in the Algorithm 1.

Algorithm 1: MOAGWO algorithm.

```
Set the basic parameters of the algorithm;
Set the input parameters of the problem and specify their
  boundaries;
Initialize the random location of Grey Wolves (X⃗);
Create an archive repository to store the non-dominated
  Wolves;
while t ≤ Max_t do
    Check the boundaries of the Wolf locations using the
      mirroring method [27];
    Generate a random value within zero to one (r_8).;
    Based on r_8 and 1 − t/Max_t decide to update the position
      using one or three leader(s);
    Randomly chose leaders from the archive;
    Update the locations (X⃗_(t+1)) using Eq. (31);
    Calculate the value of objective functions for each Wolf
      (F(X⃗));
    Update the archive by the non-dominated solutions;
    t = t + 1;
    Check the stopping criteria using Eq. (32);
end
Return the archive solutions as the set of Pareto solutions;
```

3.3. Implementation of MOAGWO into the problem

The proposed MOAGWO, to determine the Pareto front solutions comprising the near-optimal parameters of DG, ESS, SVC, and VR units for the different scenarios are shown in flowchart of Fig. 1.

4. Results and discussion

We tested the proposed formulation on IEEE 33-bus (Fig. 2) and 69-bus (Fig. 3) medium voltage test systems. The system data, load characteristics, and average DG output powers can be found in [28,34–36]. For each test system, the Pareto-optimal solutions were determined for eight scenarios to identify the ESS, SVC, and VR impacts on the objectives. Among them, the first scenario (cs-1) referred to the base-case where we maximize the DG capacity without using any additional devices. The following three scenarios were devoted to identifying the marginal impacts of ESS, SVC, and VR on the DGHC and energy losses. The last four scenarios were organized to search for the collective impact of device groups on the objective functions. The scenarios are listed in Table 1 together with available devices and corresponding control parameters ($\vec{X}$) (33). the control parameters for the different control variables are defined in Eqs. (34)–(45). The control vector and

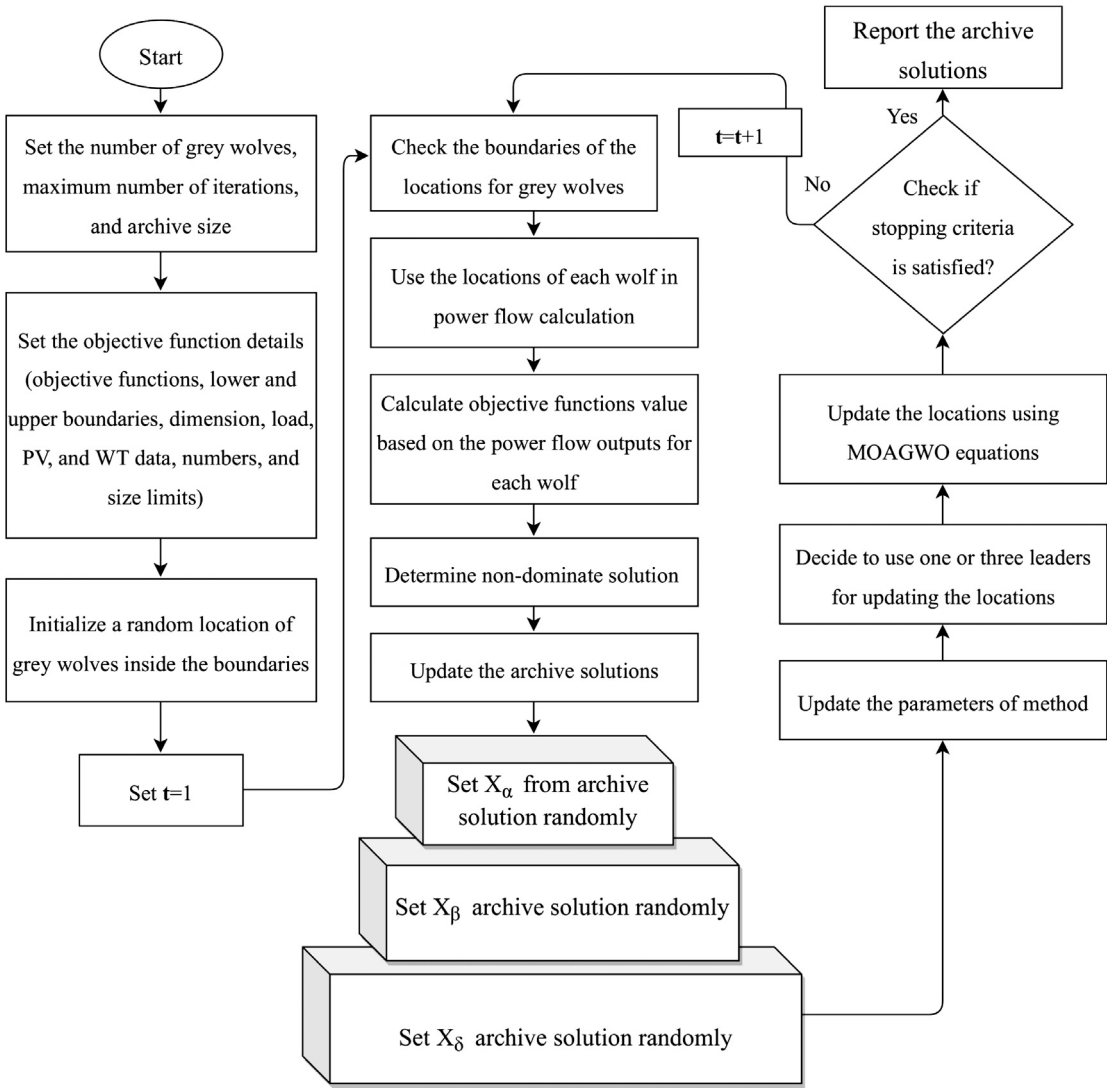

Fig. 1. MOAGWO algorithm flowchart for proposed problem.

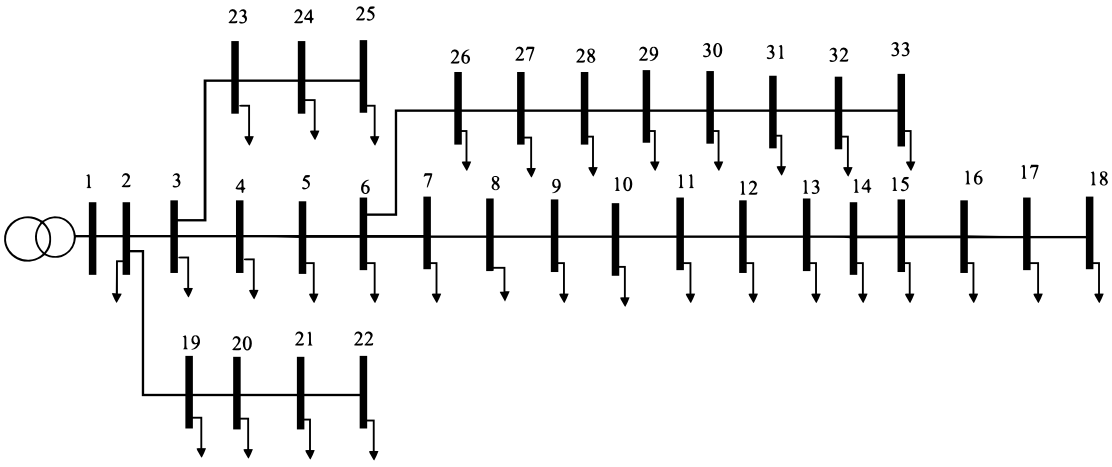

Fig. 2. EEE 33-bus test system single-line diagram.

its entries are defined below, where T denotes the transpose. Note that each scenario in the table can include different control vectors.

$$\vec{X} = \{\vec{L}, \vec{S}, \overrightarrow{Type}, \vec{E}, \vec{P}, \vec{O}, \overrightarrow{Tap}\} \tag{33}$$

The location of PV, WT, ESS, and SVC units is one of the control variables for the problem defined as follows:

$$\vec{L} = \left[L_1 \quad L_2 \quad \dots \quad L_{(N_{PV}+N_{WT}+N_{ESS}+N_{SVC})}\right]^T, \tag{34}$$

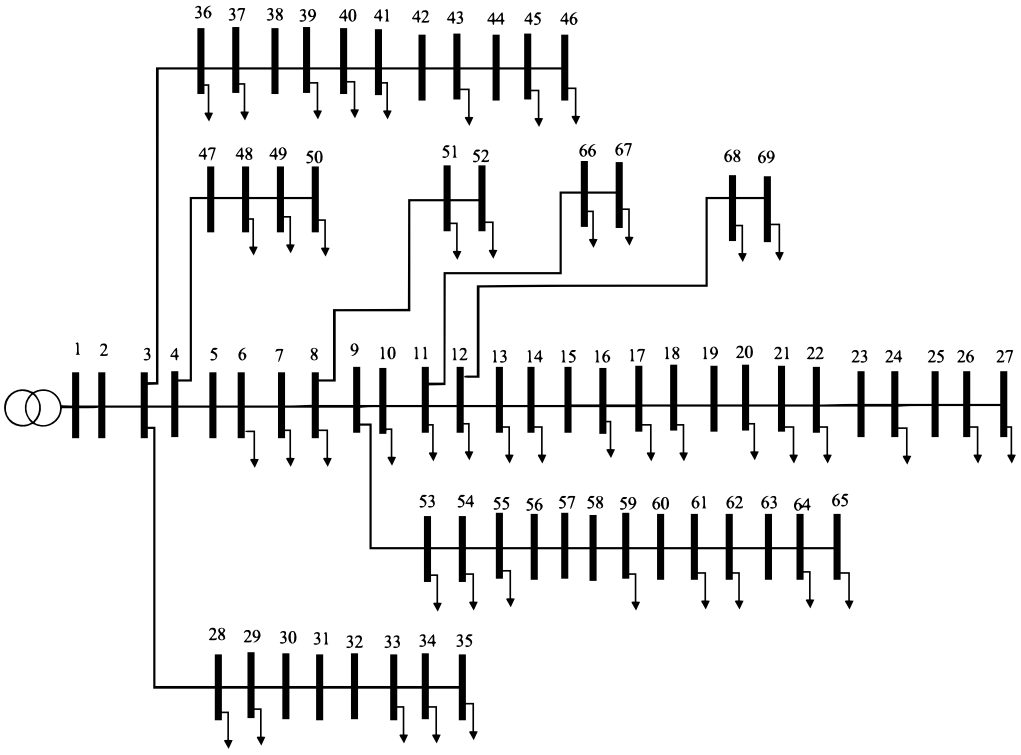

Fig. 3. 69-bus system single-line diagram.

Table 1
The list of scenarios together with available devices and corresponding control parameters.

Scenario	Devices	$\overrightarrow{X}$
cs-1	DGs	$\{\overrightarrow{L}, \overrightarrow{S}, \overrightarrow{Type}\}$
cs-2	DGs and ESSs	$\{\overrightarrow{L}, \overrightarrow{S}, \overrightarrow{Type}, \overrightarrow{E}, \overrightarrow{P}, \overrightarrow{O}\}$
cs-3	DGs and SVCs	$\{\overrightarrow{L}, \overrightarrow{S}, \overrightarrow{Type}, \overrightarrow{O}\}$
cs-4	DGs and VR	$\{\overrightarrow{L}, \overrightarrow{S}, \overrightarrow{Type}, \overrightarrow{Tap}\}$
cs-5	DGs, ESSs, and SVCs	$\{\overrightarrow{L}, \overrightarrow{S}, \overrightarrow{Type}, \overrightarrow{E}, \overrightarrow{P}, \overrightarrow{O}\}$
cs-6	DGs, SVCs, and VR	$\{\overrightarrow{L}, \overrightarrow{S}, \overrightarrow{Type}, \overrightarrow{O}, \overrightarrow{Tap}\}$
cs-7	DGs, ESSs, and VR	$\{\overrightarrow{L}, \overrightarrow{S}, \overrightarrow{Type}, \overrightarrow{E}, \overrightarrow{P}, \overrightarrow{O}, \overrightarrow{Tap}\}$
cs-8	DGs, SVCs, ESSs, and, VR	$\{\overrightarrow{L}, \overrightarrow{S}, \overrightarrow{Type}, \overrightarrow{E}, \overrightarrow{P}, \overrightarrow{O}, \overrightarrow{Tap}\}$

$$L_1, \ldots, L_{(N_{PV}+N_{WT}+N_{ESS}+N_{SVC})} \in \mathbb{Z}$$

The vector $\overrightarrow{S}$ shows size of the DG and SVC units. The dimension of the vector is equal to the sum of DG and SVC units $N_{PV}+N_{WT}+N_{SVC}$.

$$\overrightarrow{S} = \begin{bmatrix} S_1 & S_2 & \ldots & S_{(N_{PV}+N_{WT}+N_{SVC})} \end{bmatrix}^T, \quad S_1, \ldots, S_{(N_{PV}+N_{WT}+N_{SVC})} \in \mathbb{R}^+ \tag{35}$$

The types of the DG units are identified by the type vector.

$$\overrightarrow{Type} = \begin{bmatrix} Type_1 & Type_2 & \ldots & Type_{(N_{PV}+N_{WT})} \end{bmatrix}^T, \quad Type_1, \ldots, Type_{(N_{PV}+N_{WT})} \in \mathbb{Z}_2 \tag{36}$$

The scenarios comprising ESS units have additional energy capacity and maximum power control parameters besides their locations. These additional control parameters are represented by the $\overrightarrow{E}$ and $\overrightarrow{P}$ vectors given below:

$$\overrightarrow{E} = \begin{bmatrix} E_1 & E_2 & \ldots & E_{N_{ESS}} \end{bmatrix}^T, \quad E_1, \ldots, E_{N_{ESS}} \in \mathbb{R}^+ \tag{37}$$

$$\overrightarrow{P} = \begin{bmatrix} P_1 & P_2 & \ldots & P_{N_{ESS}} \end{bmatrix}^T, \quad P_1, \ldots, P_{N_{ESS}} \in \mathbb{R}^+ \tag{38}$$

The operation strategy of the ESS and SVC units and the tap positions of VRs are the last control parameters. They are defined as follows:

$$\overrightarrow{O} = \begin{bmatrix} O_{11} & O_{12} & \cdots \\ \vdots & \ddots & \\ O_{(N_{ESS}+N_{SVC})1} & & O_{(N_{ESS}+N_{SVC})N_T} \end{bmatrix}, \quad O_{11}, \ldots, O_{(N_{ESS}+N_{SVC})N_T} \in \mathbb{R} \tag{39}$$

$$\overrightarrow{Tap} = \begin{bmatrix} Tap_1 & Tap_2 & Tap_{N_T} \end{bmatrix}^T, \quad Tap_{11}, \ldots, Tap_{N_T} \in \mathbb{Z} \tag{40}$$

where the boundaries for the ith control variable are given as:

$$2 \le L_i \le N_{BUS}, \tag{41}$$

$$0 \le S_i \le (1\ \text{MW}, 0.2\ \text{MVAr}) \tag{42}$$

$$0 \le E_i \le 1\ \text{MWh}, \tag{43}$$

$$0 \le P_i \le 1\ \text{MW}, \tag{44}$$

$$-16 \le Tap_i \le 16, \tag{45}$$

4.1. IEEE 33-bus system

We applied the proposed formulation to the IEEE 33-bus test system, where the base case total energy losses was 833.2 MWh. The Pareto front solutions found by the MOAGWO algorithm for different scenarios are shown in Fig. 4.

The summary of the maximum and minimum benefits of the Pareto solution for each case scenario is shown in Table 2. Note that TDS represents the total DG size in the scenarios, TEL shows the total energy losses, and TEC is the total ESS capacity all over the system. Besides, the TSS represents the total SVC size and minimum and maximum voltage magnitude in the system shown with VM. One can easily recognize

Table 2
Summary of the result in the IEEE 33-bus test system for different scenarios.

	TDS [kW]		TEL [MWh]		VM [p.u.]		TEC [kWh]		TSS [kVAr]	
	Min.	Max.	Min.	Max.	Max.	Min.	Min.	Max.	Min.	Max.
cs-1	6850	10 980	306	484	1.02	0.95				
cs-2	6540	10 720	296	592	1.04	0.95	1350	4330		
cs-3	6680	11 120	267	567	1.04	0.95			150	458
cs-4	7040	9730	295	442	1.05	0.96				
cs-5	6950	11 600	281	669	1.04	0.95	2210	4220	130	202
cs-6	7130	7810	293	371	1.05	0.95			44	101
cs-7	6850	7730	288	343	1.05	0.95	1660	2620		
cs-8	5160	6620	288	321	1.05	0.95	2270	3570	53	112

TDS: Total DG size, TEL: total energy losses, VM: Voltage magnitude,
TEC: Total ESS capacity, TSS: Total SVC size.

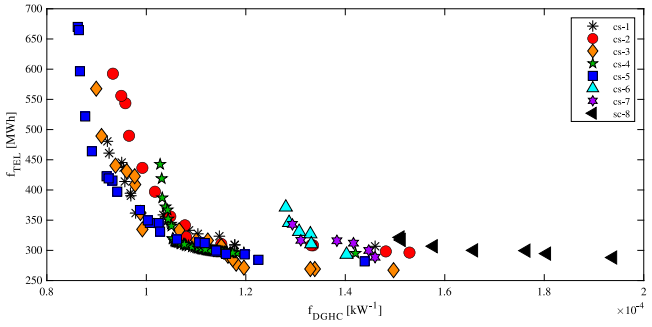

Fig. 4. Pareto front solutions for the IEEE 33-bus MV test system.

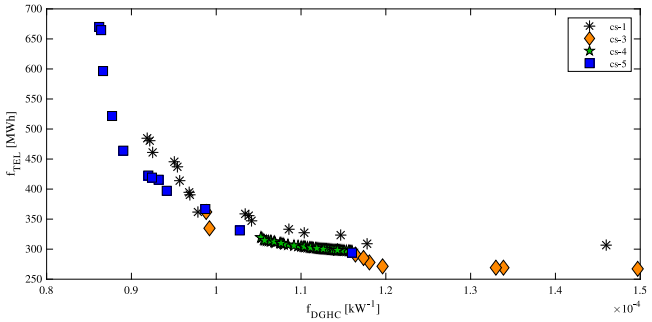

Fig. 5. The non-dominated Pareto front solutions for IEEE 33-bus test system.

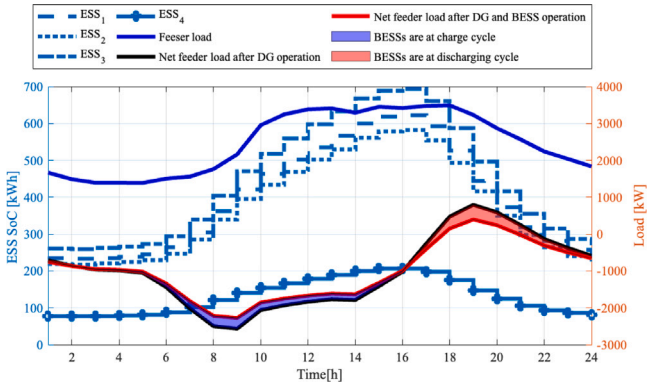

Fig. 6. SoC of ESS units and Energy transfer from/to the unit for a representative Pareto solution cs-5 in IEEE 33-bus system.

from Table 2 that the SVCs are the most effective devices to maximize the DGHC up to 11.12 MWh (cs-3), and ESSs come next. From the last four scenarios, the use of ESSs and SVCs together provides the highest DGHC, 11.6 MW (cs-5). It is also clear that VR does not improve the DGHC. On the other hand, SVCs are again the most effective devices to minimize energy losses. They can decrease annual energy losses up to 267 MWh (70%) in cs-3. Additional use of ESSs and VR does not provide any more decrease in energy losses. However, the ESSs are indispensable assets in the case of renewable DG penetration, required for the energy transfer between peak and off-peak hours. All the cases improve the minimum voltage magnitude to 0.95 p.u., which was 0.91 p.u. for the base case operating conditions in bus 18. The minimum voltage magnitudes for the non-dominated solutions shown in Fig. 4 are illustrated in Fig. A.1. The solution is for the load and DG output given in [28,34–36]. Note that the optimization processes eliminated all the undervoltages because of the lack of DGs and overvoltages because of heavy DG integration and brought them to a feasible range [0.95 - 1.05 p.u.] in all scenarios.

The non-dominated solutions for the Pareto space are re-plotted in Fig. 5 to identify the most effective devices on the DGHC. We can classify the DG penetration level into three regions without loss of generality. For the low DG penetration level up to 8.4 MW, SVCs are the most effective devices for loss minimization, which can be decreased up to 13.5% considering cs-1 values. The VR becomes the best choice for moderate DG penetration levels between 8.4 MW and 9.5 MW, where the TEL is improved up to 18.1%. Beyond this point, ESS + SVC configurations are the best alternatives for loss minimization at high DG penetration levels up to 11.6 MW. For example, 11 MW of DG penetration provides 13.4% of TEL improvements with respect to cs-1 conditions. Finally, the inclusion of VR disproves the benefits of ESS and SVC configuration.

The probability distribution of the unit (DG, ESS, SVC) locations is illustrated in Table A.1. Note that some of the nodes may accommodate more than one unit. The correlation between the DG location probabilities of cs-1 and cs-2 and cs-1 and cs-3 are 0.713 and 0.757, respectively. This indicates that the DG locations of cs-1 are not significantly affected when they are configured with ESSs and SVCs. On the other hand, the correlation between the DG location probabilities of cs-1 and cs-4 is 0.392, which indicates that the existence of VR changes the location of the installed DGs. One can infer from a similar correlation analysis that the existence of VR changes the optimal ESS and SVC locations as well. Optimal locations and sizes for a representative Pareto solution for cs-5 are illustrated in Table 3, where the total DG power output is 10.6 MW, and total energy losses are 397 MWh. The operation strategies of the ESS units to satisfy the constraint given in Eq. (13) for the load characteristics and average DG output powers defined in [28,34–36] are shown in Fig. 6.

4.2. 69-Bus system

The Pareto front solutions for the eight scenarios are shown in Fig. 7 and the range of improvements achieved by the Pareto solutions are illustrated in Table 4. ESSs are the most effective devices for this test system to maximize the DGHC (cs-2), SVCs come next, and VR is the last. When all the scenarios are thought together, ESSs itself provides the highest DGHC up to 13.27 MW (cs-2). In fact, this may

Table 3
Optimum unit locations and parameters for a representative Pareto solution of cs-5.

#	DG			ESS			SVC	
	L	S [kW]	Type	L	E [kWh]	P [kW]	L	S [kVAr]
1	4	880	WT	27	830	58	13	56
2	28	920	WT	22	1000	70	12	30
3	25	960	WT	19	510	36	29	47
4	26	970	WT	25	230	16	24	18
5	23	940	PV					
6	22	860	PV					
7	19	940	PV					
8	27	740	WT					
9	24	940	PV					
10	29	900	PV					
11	17	330	PV					
12	13	730	WT					
13	20	340	PV					
14	14	170	WT					

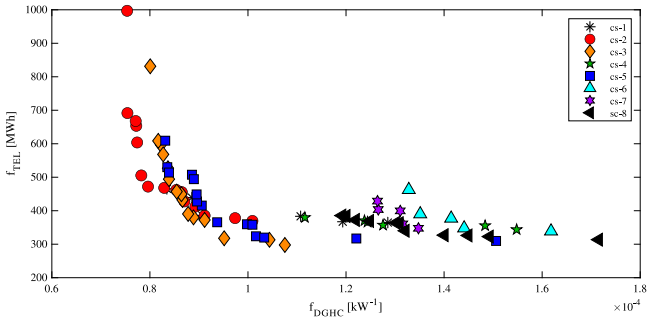

Fig. 7. Pareto front solutions for the 69-bus test system.

be misleading as the energy losses are relatively high for this extreme case. SVCs are again the most effective devices to minimize the energy losses. They can decrease it up to 297 MWh (70%) in cs-3, which was initially 989.4 MWh for the base case operating conditions. The total DG and SVC sizes for this case are 9.3 MW and 375 kVAr, respectively.

The Pareto solutions of the cs-2, cs-3, and cs-5 in Fig. 7 dominated the other scenario cases solutions. In contrast with the DG penetration levels, cs-2 dominates for high DG penetration levels where the total DG capacity is greater than 11.7 MW, cs-3 dominates for the moderate DG penetration level between 9.3 MW to 11.7 MW, and cs-5 dominates for the lower DG penetration levels.

The probability distribution of the unit locations for the Pareto solutions in each scenario case is illustrated in Table A.2. The correlation analysis did not give definite results to infer certain conclusions about the impacts of ESS, SVC, and VR installation on the DG installation probability of the system buses.

The impact of installing the different devices on the voltage profile is shown in Fig. A.2. The voltage profile improvements provided by the Pareto front solutions are illustrated in Fig. A.2 for the representative solutions of each scenario case. Note that the representative solutions are randomly selected among the ones whose TEL values are between 360 to 375 MWh. The critical voltage magnitudes, which were less than 0.95 p.u. for the base case operating conditions, belonged to the buses between 57 and 65. All of them were increased over the minimum permissible level of 0.95 p.u. for all test scenarios, while the maximum voltage magnitudes were kept at less than 1.05 p.u.

4.3. Comparison of solution algorithms

The quality of the Pareto solutions found by MOAGWO is verified by comparing the solutions with the Pareto solutions obtained by Multi-objective Particle Swarm Optimization (MOPSO) [37] and Multi-objective Grey Wolf Optimization Algorithm (MOGWO) [38]. For this purpose, the performance metrics, namely spacing metric (SM), domination percentage (DP) metric, and Hyper-volume (HV) metric, are used. The details of the metrics can be found in [32,33,39]. In addition, the computational cost of the algorithms are also compared.

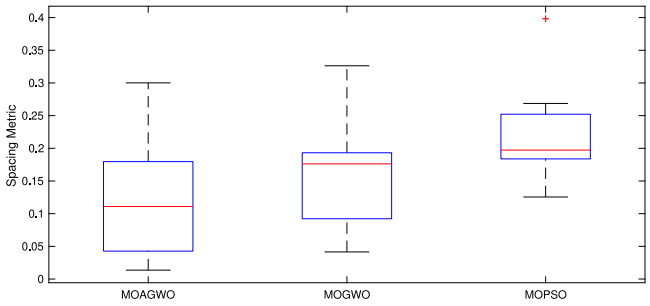

Fig. 8. The box-plots of SM values of different optimization algorithms.

As MOGWO and MOAGWO are parameter-free algorithms, the MOPSO parameters are first optimized with respect to DP metric results for different parameters before the performance comparisons. The best parameters for the MOPSO method are found as follows. The grid inflation rate is set to 0.1. The personal and global learning coefficients are set to 1. The best value of 0.95 was found for the damping ratio. Besides the mentioned parameters, the algorithm sets the number of grids per dimension and leader selection parameters to 10 and 4. The performance metrics comparison for the algorithm are as follows:

4.3.1. The spacing metric

This metric is a value estimating how evenly the non-dominated solutions are distributed in the Pareto front space. The SM evaluates the distribution of vectors throughout the set of non-dominated solutions and computes with a relative distance measure between consecutive solutions in the obtained non-dominated set. SM is defined as the standard deviation of the minimum Euclidean distances between the non-dominated solutions as given;

$$SM = \sqrt{\frac{1}{k}\sum_{i=1}^{k}(\bar{d} - d_i)^2} \tag{46}$$

where $\bar{d}$ is the average Euclidean distance,

$$\bar{d} = \frac{1}{k}\sum_{i=1}^{k} d_i \tag{47}$$

Note that the small SM values show closely-distributed solutions in the Pareto front space, indicating the higher performance of the solution algorithm.

The box plots of the SM values of the different multi-objective optimization algorithms are shown in Fig. 8. Note that each box plot represents the distribution of SM values in ten independent runs for each scenario of the study. Compared to the other two algorithms, the proposed MOAGWO method has the minimum median and minimum dispersion, which means that it shows better performance in finding the evenly distributed solutions in the Pareto solution set.

4.3.2. The domination percentage metric

The DP provides information on better convergence and quality of the solutions. For example, given two sets of the non-dominated solutions, A and B, DP(A,B) refers to the percentage of solutions in A that are dominated at least by one solution in B. DP(A,B) <DP(B,A) shows a more acceptable convergence of the A set.

Table 4
Summary of the result in 69-bus system for different cs.

	TDS [kW]		TEL [MWh]		VM [p.u.]		TEC [kWh]		TSS [kVAr]	
	Min.	Max.	Min.	Max.	Min.	Max.	Min.	Max.	Min.	Max.
cs-1	7780	11 980	364	465	1.01	0.95				
cs-2	9910	13 270	369	997	1.04	0.95	2820	5280		
cs-3	9300	12 490	297	831	1.04	0.95			255	462
cs-4	6460	8960	343	379	1.05	0.95				
cs-5	6640	12 030	309	609	1.04	0.95	4270	6560	251	466
cs-6	6180	7530	338	462	1.04	0.95			120	165
cs-7	7420	7910	347	428	1.05	0.95	2320	3460		
cs-8	5830	8390	313	385	1.05	0.95	3520	5460	81	161

TDS: Total DG size, TEL: total energy losses, VM: Voltage magnitude,
TEC: Total ESS capacity, TSS: Total SVC size.

Table 5
Comparisons of the algorithms Using DP index.

	Mean	STD	Maximum	Minimum
DP(MOAGWO,MOGWO)	21.5	28.3	85.7	0.0
DP(MOGWO,MOAGWO)	55.4	40.1	100	2.6
DP(MOAGWO,MOPSO)	9.7	18.9	76.9	0.0
DP(MOPSO,MOAGWO)	76.1	33.8	100	0.0

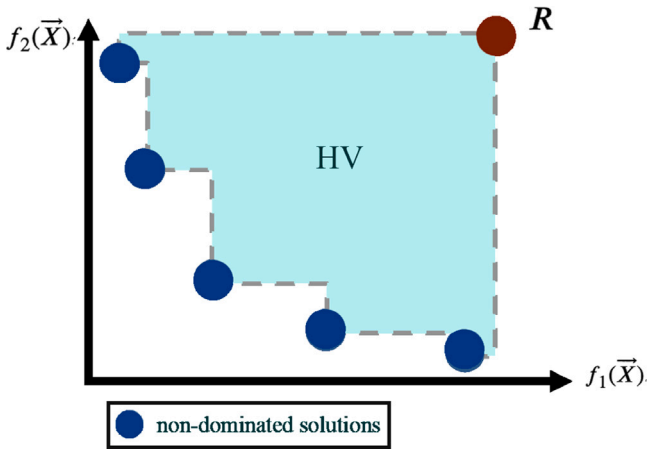

Fig. 9. The estimated HV for 2-D space.

The DP index, $DP(A, B)$ refers to the mapping the percentage of the domination to the interval [0, 100] percent and it can be calculated as:

$$DP(A,B) := \frac{|\{b \in B; \exists a \in A : a \leq b\}|}{|B|} \times 100 \tag{48}$$

where a, b are the non-dominated solutions in sets A and B. Since $DP(A, B)$ may not be equivalent to $(100 - DP(B, A))$, both $DP(A, B)$ and $DP(B, A)$ have to be calculated for better understanding of dominance of the solutions.

Table 5 shows the DP index results for both test systems. From the table, it can be seen that more than 76.1% of MOPSO solutions and 55.4% of MOGWO solutions are dominated by MOAGWO solutions. This shows that MOAGWO has found a better Pareto optimal front than the other two methods, and the algorithm has acceptable convergence.

4.3.3. The hyper-volume metric

HV was originally proposed for comparing the performance of multi-objective evolutionary algorithms (MOEAs) [32]. It computes the volume dominated by a given set of non-dominated solutions bounded by a reference point R. The HV value for a set of non-dominated solutions gives us a clear idea of the convergence and diversity of the set. The HV for a set of solutions called A that normalizes the objective values is defined as:

$$HV(A,R) = volume(\bigcup_{i=1}^{|A|} v_i) \tag{49}$$

where R is the reference point and is chosen as the maximum value for the normalized objective values. v is the hypercube whose corners are the R and all solutions in A. For an illustration of HV for a two-dimensional space, see Fig. 9. Higher values of HV mean that the solution set is closer to an optimal Pareto set and may also indicate a more uniform distribution of solutions in the objective space.

A comparison of the HV index for two sets of non-dominated solutions shows that a set that dominates another set (completely or partially) has a better (higher) HV value. The mean and standard deviations of the HV index found for the different methods are shown in Table 6. The HV results are obtained by normalizing the f_{AENS}, f_{cost}, and f_{AEL} values and setting R to (1,1,1). The result of the HV index shows that MOAGWO found a higher value and, therefore, a better solution quality than the other solutions.

Table 6
The mean and standard deviations of HV values for the algorithms.

	MOAGWO	MOGWO	MOPSO
Mean	0.89	0.83	0.71
STD	0.04	0.04	0.09

Table 7
Average execution times and corresponding standard deviations.

Case study		33-bus		
Method		MOAGWO	MOGWO	MOPSO
Execution time [s]	Mean	228	360	523
	STD	61 (26.8%)	265 (73.6%)	194 (37.1%)
Case study		69-bus		
Method		MOAGWO	MOGWO	MOPSO
Execution time [s]	Mean	344	358	362
	STD	68 (19.8%)	89 (24.9%)	85 (23.5%)

4.3.4. Computational cost

The computational efficiency of the proposed algorithm is affected by the second termination criterion of the process. The computation performance of the algorithms with respect to ten runs is illustrated in Table 7. The results show that the MOAGWO algorithm is fast due to the smaller number of iterations. Moreover, it shows the smallest standard deviations, indicating that its solutions are more evenly distributed than the others.

5. Conclusions

This paper has presented a multi-objective optimization framework to maximize the DGHC while optimizing the energy losses and peak

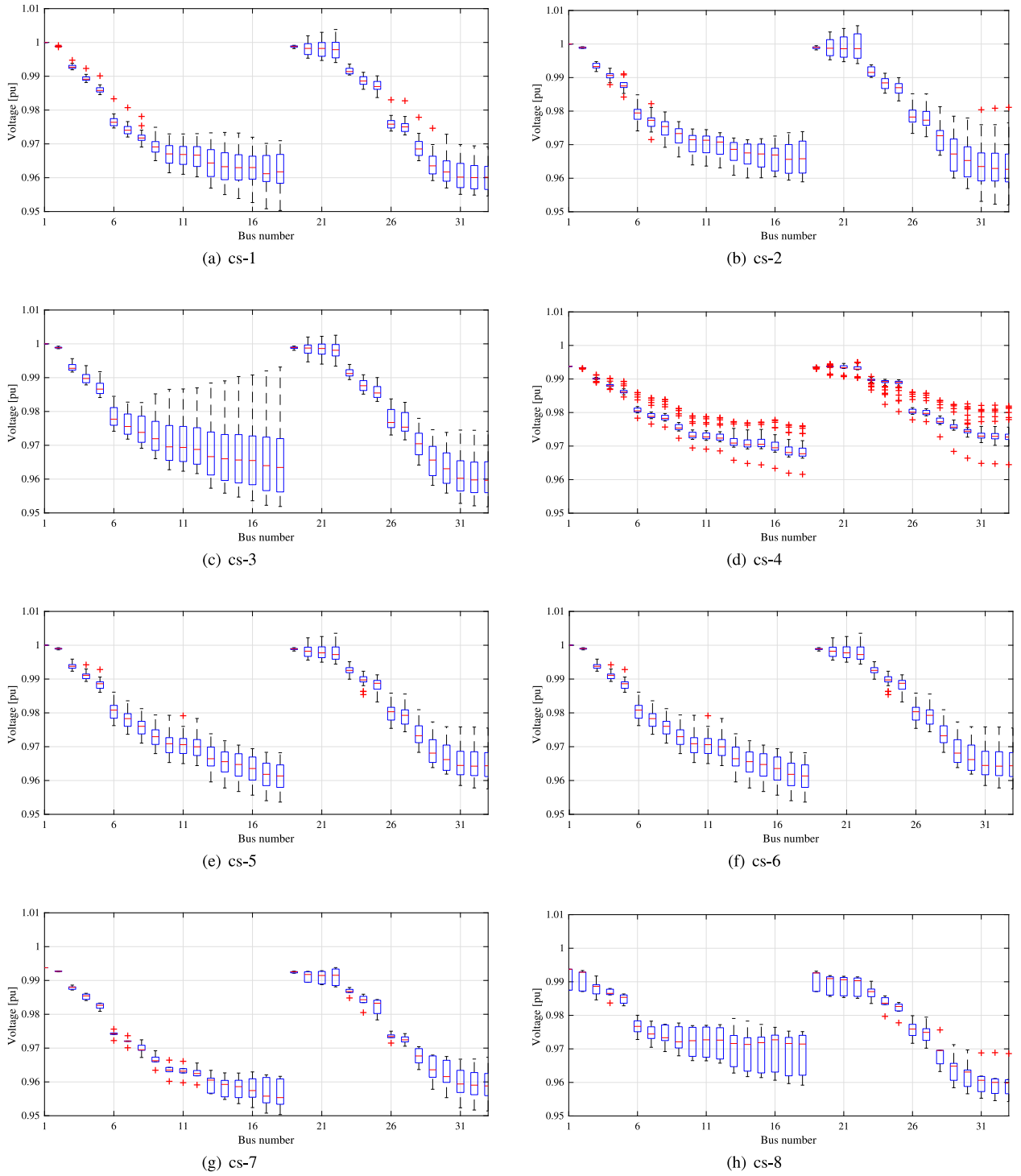

Fig. A.1. The minimum voltage magnitude for the Pareto solutions of IEEE 33-bus system.

period energy transfer. The number, size, and location of the two popular DG units, PV and WTs, were optimized at first within the multi-objective optimization cycle. Then, ESSs, VRs, and SVCs were considered for the reinforcement of the EDN to improve the objectives. Different scenarios based on the single and collaborative use of reinforcement devices were organized to determine the impact of ESS, VR, and SVC units on the objectives.

Among several Heuristic optimization algorithms, the Multi-objective Advanced Grey Wolf Optimization (MOAGWO) was used to determine the Pareto front solutions since it was the improved version of traditional GWO in search capability and convergence performances. The proposed multi-objective formulation and the solution algorithm were tested on IEEE-33-bus and 69-bus test systems.

The results showed that the optimal device type and location depend on the level of DG penetration. In this context, the impacts of the singular and collaborative reinforcement devices on the hosting capacity and the other objectives were identified, and optimal

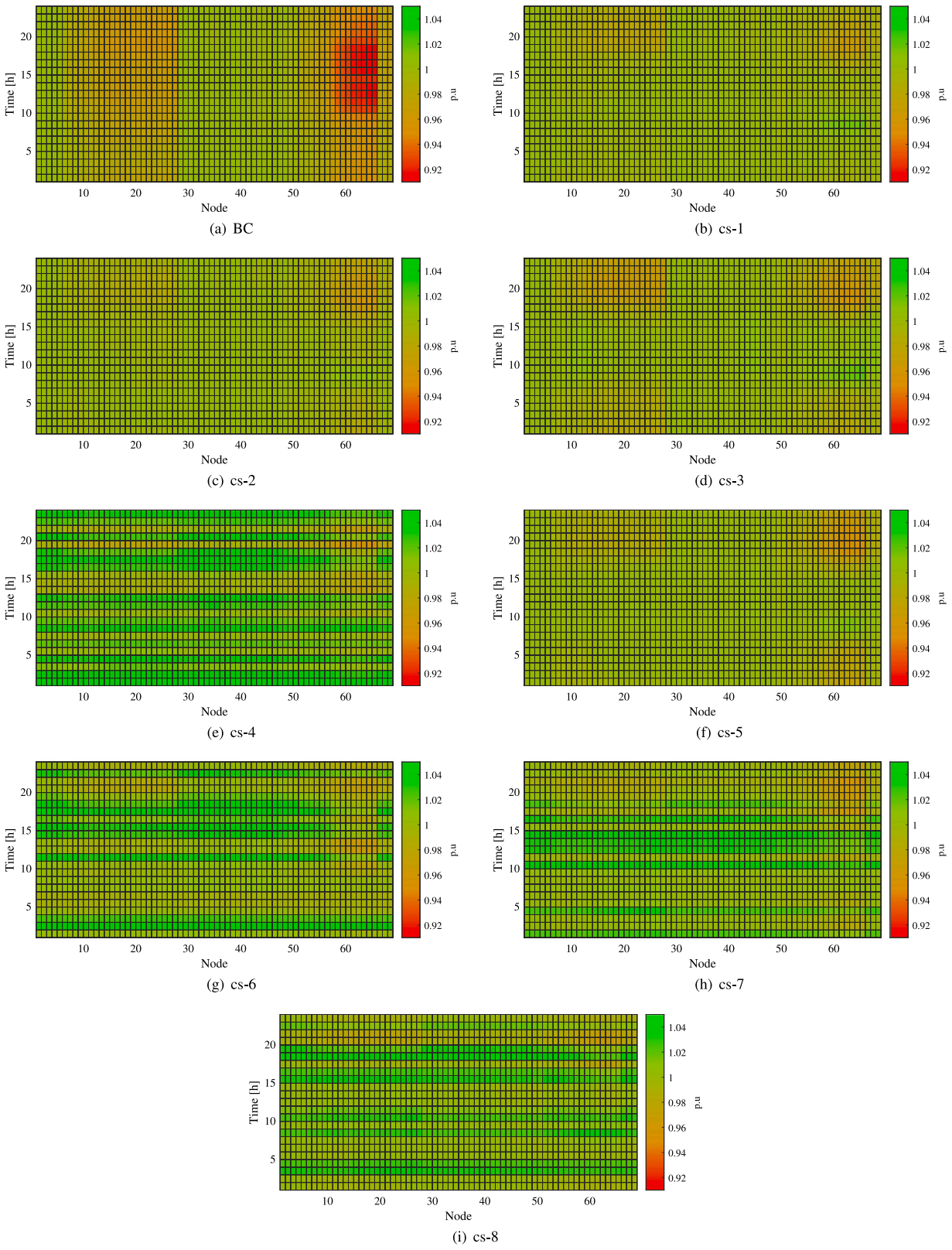

Fig. A.2. The voltage profiles for the Pareto solutions of 69-bus system.

configurations were proposed for several DG penetration levels. Moreover, the probability distribution of the DGs and reinforcement units and their inter-correlations were analyzed to guide prospective future investments on the EDN.

Finally, the performance of the proposed MOAGWO algorithm was validated by comparing its Pareto solution distributions and computational efficiency with the two other popular heuristic methods, MOPSO and MOGWO. According to the two performance metrics, the Pareto

Table A.1
The probability of installing the units in IEEE 33-bus system buses for different Pareto solutions.

Bus #		2	3	4	5	6	7	8	9	10	11	12	13	14	15	16	17	18	19	20	21	22	23	24	25	26	27	28	29	30	31	32	33
cs-1	DG	59	47	12	6	12	35	12	12	6	6	29	29	24	24	18	18	29	82	65	53	59	76	100	94	35	71	35	41	24	53	53	24
cs-2	DG	36	29	21	21	14	14	29	21	29	29	14	7	21	43	14	21	43	64	50	71	50	57	71	93	79	43	64	29	29	29	57	29
	ESS	7	21	14	21	14	0	29	21	50	7	14	14	43	29	36	14	36	21	21	21	43	21	43	50	43	36	29	43	14	29	14	0
cs-3	DG	15	25	20	25	25	10	25	20	30	35	15	15	25	30	25	10	40	70	60	55	50	70	80	90	55	35	50	35	30	40	30	15
	SVC	0	0	0	0	0	0	5	5	10	5	10	30	25	30	20	15	30	5	15	15	5	15	10	20	10	20	15	25	35	50	30	15
cs-4	DG	0	86	14	0	0	0	100	3	95	1	1	0	0	89	11	0	3	95	70	15	18	31	99	98	70	6	0	95	6	5	91	4
cs-5	DG	9	5	18	23	50	18	9	5	23	23	18	41	23	23	9	14	18	86	68	59	50	77	91	100	64	55	77	32	27	23	64	14
	ESS	5	5	9	18	18	0	5	5	0	5	18	18	14	41	32	36	23	45	45	23	36	64	23	41	50	27	55	55	27	23	18	18
	SVC	0	0	5	0	5	0	0	9	5	18	9	50	36	32	23	9	14	9	0	9	14	9	32	5	27	9	5	9	9	23	9	9
cs-6	DG	17	17	83	17	67	33	33	17	0	17	0	17	0	17	50	17	0	17	17	0	50	17	100	67	0	17	33	67	50	17	17	33
	SVC	0	0	50	33	33	50	0	17	33	0	17	0	33	0	0	0	0	0	0	17	0	17	50	17	17	0	0	0	17	0	0	0
cs-7	DG	0	0	0	17	0	17	17	0	17	17	50	33	0	17	33	33	17	67	50	50	33	50	100	83	33	83	17	67	50	67	33	0
	ESS	0	17	17	0	17	50	0	33	17	0	33	17	33	17	50	33	17	17	17	33	17	33	50	17	33	50	0	33	67	67	17	0
cs-8	DG	14	14	14	0	0	0	57	14	14	43	0	29	14	14	43	0	29	29	14	0	14	71	43	71	14	14	29	29	29	57	14	29
	ESS	0	14	14	14	29	29	14	14	0	29	29	43	0	14	43	14	43	43	14	57	29	43	57	0	14	14	43	57	29	14	29	14
	SVC	0	0	0	0	0	0	14	0	14	29	14	14	0	14	14	14	29	14	14	14	0	14	29	14	14	29	14	14	14	0	0	14

Table A.2
The probability of installing the units in 69-bus system buses for different Pareto solutions.

Bus #	cs-1	cs-2		cs-3		cs-4	cs-5			cs-6		cs-7		cs-8			Bus #	cs-1	cs-2		cs-3		cs-4	cs-5			cs-6		cs-7		cs-8		
	DG	DG	ESS	DG	SVC	DG	DG	ESS	SVC	DG	SVC	DG	ESS	DG	ESS	SVC		DG	DG	ESS	DG	SVC	DG	DG	ESS	SVC	DG	SVC	DG	ESS	DG	ESS	SVC
2	0	0	0	0	0	0	0	0	0	20	0	0	0	0	0	0	36	67	40	20	27	13	33	33	7	0	0	0	60	0	0	9	0
3	0	7	0	0	0	0	7	0	0	0	0	0	0	0	9	0	37	50	53	33	13	0	17	20	13	0	0	0	20	20	9	55	18
4	0	0	0	0	0	0	0	0	0	0	0	0	0	0	9	0	38	50	20	7	27	0	0	20	0	7	0	0	20	0	0	9	9
5	0	0	7	0	0	0	0	7	0	0	0	20	40	0	0	0	39	0	27	13	27	0	33	27	13	0	0	0	0	20	9	9	0
6	0	0	0	0	0	0	7	7	0	0	20	0	40	18	0	0	40	0	60	13	53	0	17	33	7	0	0	0	40	0	0	9	9
7	0	7	0	7	0	0	0	7	0	0	20	40	20	0	0	0	41	0	20	7	13	7	0	47	40	20	20	20	0	0	0	18	9
8	0	0	0	13	0	0	0	0	0	20	40	20	0	9	0	0	42	50	20	27	33	20	0	20	0	13	0	20	20	40	9	0	9
9	0	0	0	7	0	33	7	7	0	20	20	0	0	0	0	0	43	17	27	13	20	33	17	33	13	13	40	0	0	20	9	9	9
10	0	13	0	0	0	0	0	0	0	0	0	20	0	18	0	0	44	17	13	7	13	7	33	20	33	13	0	0	0	20	9	0	0
11	0	0	0	0	0	0	0	13	0	40	0	0	0	0	0	0	45	0	13	13	40	13	0	27	0	7	0	40	20	40	18	18	0
12	0	0	0	0	0	17	0	20	0	20	0	60	0	18	0	0	46	17	33	27	60	20	0	7	7	7	20	20	20	20	9	0	9
13	0	7	7	0	0	0	13	7	0	0	0	20	0	18	9	0	47	33	60	27	27	0	0	33	13	7	20	0	0	40	9	18	9
14	0	7	0	0	0	0	0	13	7	0	0	0	0	9	0	0	48	33	20	20	53	0	17	47	13	7	20	60	60	20	18	9	0
15	17	7	7	13	0	17	7	7	0	0	0	0	0	0	18	0	49	83	40	13	33	0	17	53	20	0	0	0	20	0	18	27	0
16	0	27	7	0	0	33	0	0	0	0	0	0	0	0	0	0	50	33	60	20	47	13	33	53	13	7	20	0	40	20	55	0	0
17	17	7	7	7	0	0	0	7	7	0	0	0	20	9	0	9	51	33	33	20	33	13	17	20	13	7	20	0	0	20	36	0	0
18	0	7	0	0	0	0	0	0	0	40	0	20	0	9	27	0	52	50	20	13	13	20	33	27	27	7	20	0	0	0	0	9	0
19	0	13	0	0	0	17	0	7	0	0	0	20	0	0	27	0	53	17	47	13	20	7	33	13	7	13	0	20	0	40	9	9	18
20	17	0	13	0	0	17	13	7	0	20	0	0	0	0	0	0	54	0	20	33	40	13	17	0	13	7	0	20	20	20	27	27	18
21	33	0	13	0	0	17	0	7	0	0	0	0	0	0	9	0	55	17	7	13	33	13	17	7	20	7	20	0	40	0	9	18	0
22	0	13	0	13	0	17	0	13	7	40	0	0	0	9	18	9	56	17	20	33	13	7	50	33	13	20	0	0	0	20	27	18	0
23	0	13	20	7	0	17	7	0	0	0	0	0	0	0	9	9	57	17	33	7	47	27	17	33	27	27	0	0	0	40	0	27	9
24	0	0	0	7	7	0	0	7	0	0	0	0	0	0	18	0	58	33	40	40	33	27	33	27	20	13	0	0	0	0	27	18	0
25	0	0	13	0	0	0	0	7	0	0	0	20	0	18	18	0	59	0	60	7	27	0	67	33	7	47	60	0	0	0	36	9	9
26	17	0	7	0	7	0	13	7	7	0	20	0	0	0	27	0	60	100	33	27	47	13	33	33	13	40	40	20	40	0	55	9	27
27	0	7	0	13	7	0	0	13	7	0	0	0	0	0	9	0	61	83	53	13	33	27	67	53	27	20	80	0	60	20	55	18	9
28	33	20	0	0	0	33	27	13	7	40	0	0	0	18	18	9	62	33	33	33	73	47	33	73	13	27	20	20	60	40	45	0	18
29	0	20	7	27	0	33	7	0	0	0	0	0	40	9	27	0	63	67	53	13	53	27	50	40	33	27	20	20	60	20	55	9	18
30	0	20	13	20	0	0	7	0	0	20	0	20	0	0	0	0	64	50	47	13	33	33	50	47	27	13	60	0	60	40	64	36	27
31	50	20	13	13	7	33	40	0	13	0	0	0	0	27	18	27	65	50	40	7	53	20	67	47	33	13	60	20	0	20	36	18	27
32	33	20	13	47	0	17	13	0	0	20	0	20	0	0	18	0	66	33	20	40	33	20	0	33	20	27	20	0	20	20	27	18	0
33	0	13	7	7	0	50	20	7	7	0	0	0	0	18	9	0	67	17	20	27	27	20	17	40	27	13	0	0	0	20	27	27	18
34	0	20	7	13	7	17	0	20	7	0	0	0	0	0	9	0	68	0	13	13	27	27	33	47	33	0	0	0	0	40	18	0	36
35	0	20	13	13	0	0	7	7	0	0	0	0	20	0	18	0	69	17	27	0	13	7	0	7	27	7	0	0	20	0	18	9	0

front distribution obtained by MOAGWO was found to be the best. Moreover, MOAGWO was the fast computation algorithm, providing more even in computation times.

CRediT authorship contribution statement

Bahman Ahmadi: Investigation, Software development, Writing – original draft, Visualization. **Oguzhan Ceylan:** Methodology, Data curation, Writing – review & editing, Formal analysis. **Aydogan Ozdemir:** Conceptualization, Writing – review & editing, Validation, Supervision, Project administration.

Declaration of competing interest

The authors declare that they have no known competing financial interests or personal relationships that could have appeared to influence the work reported in this paper.

Data availability

Data will be made available on request.

Acknowledgments

This research funded as a part of "117E773 Advanced Evolutionary Computation for Smart Grid and Smart Community" project under the framework of 1001 Project organized by "The Scientific and Technological Research Council of Turkey TUBITAK" and "EU HORIZON 2020 – Sustainable and Integrated Energy Systems in Local Communities (SERENE)".

Appendix

See Figs. A.1, A.2 and Tables A.1, A.2.

References

[1] M. Faheem, M.W. Ashraf, R.A. Butt, B. Raza, M.A. Ngadi, V.C. Gungor, Ambient energy harvesting for low powered wireless sensor network based smart grid applications, in: 2019 7th International Istanbul Smart Grids and Cities Congress and Fair (ICSG), IEEE, 2019, pp. 26–30.

[2] M. Faheem, M. Umar, R.A. Butt, B. Raza, M.A. Ngadi, V.C. Gungor, Software defined communication framework for smart grid to meet energy demands in smart cities, in: 2019 7th International Istanbul Smart Grids and Cities Congress and Fair (ICSG), IEEE, 2019, pp. 51–55.

[3] S. Khan, P. Zehetbauer, R. Schwalbe, Evaluation of sensitivity based coordinated volt-var control and local reactive power for voltage regulation and power exchange across system boundaries in smart distribution networks, Electr. Power Syst. Res. 192 (2021) 106975.

[4] Y. Yao, F. Ding, K. Horowitz, A. Jain, Coordinated inverter control to increase dynamic PV hosting capacity: A real-time optimal power flow approach, IEEE Syst. J. (2021).

[5] K. Luo, W. Shi, Comparison of voltage control by inverters for improving the PV penetration in low voltage networks, IEEE Access 8 (2020) 161488–161497.

[6] Y. Mu, T. Yao, H. Jia, X. Yu, B. Zhao, X. Zhang, C. Ni, L. Du, Optimal scheduling method for belt conveyor system in coal mine considering silo virtual energy storage, Appl. Energy 275 (2020) 115368.

[7] B. Wang, C. Zhang, Z.Y. Dong, X. Li, Improving hosting capacity of unbalanced distribution networks via robust allocation of battery energy storage systems, IEEE Trans. Power Syst. 36 (3) (2020) 2174–2185.

[8] P.H. Divshali, L. Söder, Improving PV dynamic hosting capacity using adaptive controller for STATCOMs, IEEE Trans. Energy Convers. 34 (1) (2018) 415–425.

[9] S. Lakshmi, S. Ganguly, Modelling and allocation planning of voltage-sourced converters to improve the rooftop PV hosting capacity and energy efficiency of distribution networks, IET Gener., Transm. Distrib. 12 (20) (2018) 4462–4471.

[10] R. Gupta, F. Sossan, M. Paolone, Countrywide PV hosting capacity and energy storage requirements for distribution networks: The case of Switzerland, Appl. Energy 281 (2021) 116010.

[11] M. Bajaj, A.K. Singh, Optimal design of passive power filter for enhancing the harmonic-constrained hosting capacity of renewable DG systems, Comput. Electr. Eng. 97 (2022) 107646.

[12] M.S.S. Abad, J. Ma, Photovoltaic hosting capacity sensitivity to active distribution network management, IEEE Trans. Power Syst. 36 (1) (2020) 107–117.

[13] D. Chathurangi, U. Jayatunga, S. Perera, A. Agalgaonkar, T. Siyambalapitiya, A nomographic tool to assess solar PV hosting capacity constrained by voltage rise in low-voltage distribution networks, Int. J. Electr. Power Energy Syst. 134 (2022) 107409.

[14] X. Luo, Y. Liu, P. Feng, Y. Gao, Z. Guo, Optimization of a solar-based integrated energy system considering interaction between generation, network, and demand side, Appl. Energy 294 (2021) 116931.

[15] J. Lee, J.-P. Bérard, G. Razeghi, S. Samuelsen, Maximizing PV hosting capacity of distribution feeder microgrid, Appl. Energy 261 (2020) 114400.

[16] D. Liu, C. Wang, F. Tang, Y. Zhou, Probabilistic assessment of hybrid wind-PV hosting capacity in distribution systems, Sustainability 12 (6) (2020) 2183.

[17] D. Liu, C. Zhang, Y. Xu, Z. Dong, Y. Chi, Sensitivity region based optimization for maximiz-ing renewable generation hosting capacity of an islanded microgrid, IEEE Trans. Smart Grid (2022).

[18] E.C. da Silva, O.D. Melgar-Dominguez, R. Romero, Simultaneous distributed generation and electric vehicles hosting capacity assessment in electric distribution systems, IEEE Access 9 (2021) 110927–110939.

[19] X. Cao, T. Cao, F. Gao, X. Guan, Risk-averse storage planning for improving RES hosting capacity under uncertain siting choice, IEEE Trans. Sustain. Energy (2021).

[20] M. Magdy, M. Elshahed, D.K. Ibrahim, Enhancing PV hosting capacity using smart inverters and time of use tariffs, Iran. J. Sci. Technol., Trans. Electr. Eng. (2021) 1–16.

[21] A. Ali, K. Mahmoud, M. Lehtonen, Enhancing hosting capacity of intermittent wind turbine systems using bi-level optimisation considering OLTC and electric vehicle charging stations, IET Renew. Power Gener. 14 (17) (2020) 3558–3567.

[22] R. Tanabe, H. Ishibuchi, An analysis of quality indicators using approximated optimal distributions in a 3-D objective space, IEEE Trans. Evol. Comput. 24 (5) (2020) 853–867.

[23] Y. Li, B. Feng, G. Li, J. Qi, D. Zhao, Y. Mu, Optimal distributed generation planning in active distribution networks considering integration of energy storage, Appl. Energy 210 (2018) 1073–1081.

[24] S.I. Taheri, M.B. Salles, A.B. Nassif, Distributed energy resource placement considering hosting capacity by combining teaching–learning-based and honey-bee-mating optimisation algorithms, Appl. Soft Comput. 113 (2021) 107953.

[25] B. Ahmadi, O. Ceylan, A. Ozdemir, Enhancing photovoltaic hosting capacity in distribution networks by optimal allocation and operation of static var compensators, in: 2022 57th International Universities Power Engineering Conference (UPEC), IEEE, 2022, pp. 1–6.

[26] Q. Qi, C. Long, J. Wu, K. Smith, A. Moon, J. Yu, Using an MVDC link to increase DG hosting capacity of a distribution network, Energy Procedia 142 (2017) 2224–2229.

[27] B. Ahmadi, S. Younesi, O. Ceylan, A. Ozdemir, An advanced Grey Wolf Optimization Algorithm and its application to planning problem in smart grids, Soft Comput. 26 (8) (2022) 3789–3808.

[28] B. Ahmadi, O. Ceylan, A. Ozdemir, Distributed energy resource allocation using multi-objective grasshopper optimization algorithm, Electr. Power Syst. Res. 201 (2021) 107564.

[29] O. Ceylan, G. Liu, Y. Xu, K. Tomsovic, Distribution system voltage regulation by distributed energy resources, in: 2014 North American Power Symposium (NAPS), IEEE, 2014, pp. 1–5.

[30] M.A. Tawhid, V. Savsani, Multi-objective sine-cosine algorithm (MO-SCA) for multi-objective engineering design problems, Neural Comput. Appl. 31 (2) (2019) 915–929.

[31] S. Mirjalili, S.M. Mirjalili, A. Lewis, Grey wolf optimizer, Adv. Eng. Softw. 69 (2014) 46–61.

[32] B. Ahmadi, O. Ceylan, A. Ozdemir, M. Fotuhi-Firuzabad, A multi-objective framework for distributed energy resources planning and storage management, Appl. Energy 314 (2022) 118887.

[33] B. Ahmadi, O. Ceylan, A. Ozdemir, A multi-objective optimization evaluation framework for integration of distributed energy resources, J. Energy Storage 41 (2021) 103005.

[34] S. Pfenninger, I. Staffell, Long-term patterns of European PV output using 30 years of validated hourly reanalysis and satellite data, Energy 114 (2016) 1251–1265.

[35] I. Staffell, S. Pfenninger, Using bias-corrected reanalysis to simulate current and future wind power output, Energy 114 (2016) 1224–1239.

[36] B. Ahmadi, O. Ceylan, A. Özdemir, Grey wolf optimizer for allocation and sizing of distributed renewable generation, in: 2019 54th International Universities Power Engineering Conference (UPEC), IEEE, 2019, pp. 1–6.

[37] V. Trivedi, P. Varshney, M. Ramteke, A simplified multi-objective particle swarm optimization algorithm, Swarm Intell. (2019) 1–34.

[38] S. Mirjalili, S. Saremi, S.M. Mirjalili, L.d.S. Coelho, Multi-objective grey wolf optimizer: a novel algorithm for multi-criterion optimization, Expert Syst. Appl. 47 (2016) 106–119.

[39] K. yan Liu, W. Sheng, Y. Liu, X. Meng, Y. Liu, Optimal sitting and sizing of DGs in distribution system considering time sequence characteristics of loads and DGs, Int. J. Electr. Power Energy Syst. 69 (2015) 430–440.

Bahman Ahmadi received his M.Sc. degree in Electrical engineering from Istanbul Technical University, Istanbul, Turkey in 2021. He is currently a Ph.D. in Twente University, Enschede, Netherlands. His current research interests include energy management, meta-heuristics optimization algorithm and smart grid.

Oguzhan Ceylan received the M.Sc. and Ph.D. degrees in computational science and engineering from Istanbul Technical University, Istanbul, Turkey, in 2003 and 2012, respectively. From 2013 to 2015, he was a Postdoctoral Researcher with the University of Tennessee, Knoxville, TN, USA . His research interests include smart grids, integration of renewable into distribution systems, and intelligent optimization methods.

Aydogan Ozdemir was born in Artvin, Turkey in January 1957. He received B.Sc., M.Sc., and Ph.D. degrees in electrical engineering from Istanbul Technical University, Istanbul, Turkey in 1980, 1982, and 1990, respectively. He is currently a full-time professor at the same university and the manager of Fuat Kulunk High Voltage Laboratory. His current research interests are in the area of high voltage engineering and electric power systems with an emphasis on reliability assessment and intelligent system applications.